Research Article Vol. 33, No. 5 / 10 Mar 2025 / Optics Express 10069
Optics EXPRESS

Reconfigurable NIR-emission gain via thermal control in multimode tri-doped tellurite fiber

D. H. SPADOTI,[1,†,*] I. C. PINTO,[2,†] V. A. G. RIVERA,[3,†] AND Y. MESSADDEQ[2,4,†]

[1]*Telecommunications Lab at Federal University of Itajuba, 1303 Av. BPS, Itajubá 37500, Brazil*
[2]*Centre d'Optique Photonique et Lasers, Pavillon d'Optique-Photonique, Laval University, 2375 rue de la Terrasse, Quebec G1V 0A6, Canada*
[3]*Instituto de Física de São Carlos, Universidade de São Paulo, Caixa Postal 369, São Carlos, SP, Brazil*
[4]*Instituto de Quimica, Araraquara, SP 14801, Brazil*
[†]All authors contributed equally to this work.
[*]*spadoti@unifei.edu.br*

Abstract: In fiber-based telecommunication systems, information is transmitted over wide optical spectrum bands. However, the volume of data, service demands, and traffic speeds keep rising, overloading the whole fiber links. Thus, enhancing efficiency and broadening transparency are essential in optical systems. Moreover, preserving gain across the broad spectrum remains a significant bottleneck to be overcome. Here we enhance intensity and broaden emission in the C-, L- and U- telecommunication bands via thermal population control in 30 cm of a tri-doped (Er^{3+}-Tm^{3+}-Yb^{3+}) multimode tellurite fiber (3Dp-MM-Te-fiber). The results indicate that increasing the temperature, a blue shift occurs around 1530 nm, and due to energy transfer among the tri rare-earths dopants a flat gain in the near-infrared region up to 1550 nm to 1650 nm is observed with a bandwidth of more than 100 nm. Furthermore, pumping the fiber at 980 nm with a 0.1 mW signal at 1550 nm, an experimental relative gain of approximately 2.5 dB was also demonstrated at a 120 °C heating temperature.

1. Introduction

Glass matrices other than silica-based systems have been investigated, particularly those that exhibit a wide transparency range across the electromagnetic spectrum. This research is driven by the increasing demand for higher data rates and bandwidth in modern telecommunication systems, especially due to the increase of Internet of Things (IoT) devices and the implementation of optical solutions in XHaul convergent 5G/6G access networks [1,2]. Telluride based-glasses have garnered significant attention in this scenario [3], meanwhile, this special glass presents intrinsic transparent properties that enable use across a broad spectrum, including not only conventional telecommunication bands but also extending for NIR (~ 0.75–2.5 μm) and mid-infrared (MIR > 2.5–25.0 μm) bands [4]. Moreover, tellurite-based glasses present a refractive index of around 2.0, making them an excellent host for a wider variety of glass compositions, such as rare earth ions, enhancing optical properties and performance in fiber optics links as well as laser applications [5–8].

At the same time, trivalent rare-earths (REs) dopants have also been extensively investigated, especially for their potential to improve telecommunications systems and for applications in developing new devices, such as lasers, and amplifiers, among others [5,6]. In this scenario, Er^{3+}, Yb^{3+}, and Tm^{3+} have drawn significant attention as dopants in tellurite glasses, due to such intrinsic absorption regions. When properly pumped, these dopants can effectively emit in the desired telecommunication standard bands [9–11]. For instance, an experimental study conducted by Li et al. [7] demonstrated that Er^{3+} and Tm^{3+} co-doped tellurite glass can produce a flat and broad fluorescence spectral region ranging from ~1350 to 1650 nm through spontaneous radiative

#551978 https://doi.org/10.1364/OE.551978
Journal © 2025 Received 13 Dec 2024; revised 26 Jan 2025; accepted 30 Jan 2025; published 26 Feb 2025

Optics EXPRESS

transition. Theoretically, this co-doped system can also achieve an optical gain of approximately 10 dB across a broad NIR spectral range. Additionally, metallic nanoparticles, such as gold and silver, were used to enhance the local electromagnetic field around the Er^{3+} and Tm^{3+} ions in tellurite glass, thereby broadening the emission bands [8]. In a tri-doping Er^{3+}/Tm^{3+}/Nd^{3+} tellurite glass, Xia et al. [9] showed an ultra-wide and flat NIR band luminescence ranging from 1300 to 1650 nm.

Thus, according to our published paper [10], it is possible to extend the amplification range of current optical amplifiers to simultaneously cover the C-, L- and U- telecommunication bands by using a tri-doped system with Er^{3+}, Yb^{3+}, and Tm^{3+} in tungsten-tellurite glasses. The flatter broadband emission in NIR could be obtained due to the dopant Tm^{3+} presence, which receives energy transferred from Er^{3+} and Yb^{3+}, thereby enhancing the emission band up to 1560 nm, as described in the electronic energy levels transfer system in the tri-doped system.

Likewise, the temperature also influences the luminescent process in REs-doped materials, which have been extensively investigated in the last few years [10–12]. While some thermal effects are governed by classical Maxwell-Boltzmann functions, a deeper analysis of energy level interactions in the REs reveals phenomena such as Stark effects, which are better described by the Fermi-Dirac distribution, as demonstrated in [13]. Thus, temperature variations can alter both upconversion and downconversion, leading to blueshift or redshift spectrum displacement or even expanded broadband, covering from UV to NIR regions, and enhancing the emission intensity.

According to the literature, RE absorption/emission processes can arise from different effects [14]. As discussed in [13], the principles process are: (a) Re-absorption processes, which implies repeated absorption and emission processes [15]; (b) Cross-relaxation processes, where neighboring ions in the same excited state interact, with the donor ion transferring energy to the acceptor [16]. This energy transfer promotes the acceptor to a higher energy level while the donor relaxes to the ground state; (c) Excited state absorption [17], the process involves the absorption of a photon pumped at 980 nm by Er^{3+} ions, resulting in the $^4I_{11/2} \rightarrow {}^4F_{7/2}$ or $^4I_{15/2} \rightarrow {}^4I_{11/2}$ transition due to the matching energy of these energy levels with the energy of the pumped photon; (d) The site-to-site variations around the Er^{3+} ion modify the local site symmetry and thus ligand field strengths [18], leading to an inhomogeneously broadened emission spectrum; and (e) The non-resonant energy transfer between sub-levels of the Er^{3+} ions can, under thermal modifications, contributes to a gradual increment of the population in the Stark sublevels. As a result, different emission lineshape spectra can be observed compared to the absorption spectra. Therefore, the actual emission line shape depends on which effect is dominant. For instance, Fig. 1 illustrates the thermal effect on the electronic population in the Stark levels considering the distribution function of Fermi-Dirac.

In this work, we developed an experimental demonstration of temperature-controlled population dynamics in Stark levels which can enhance intensity and broaden emission across C-, L- and U-bands in a tri-doped (Er^{3+}-Tm^{3+}-Yb^{3+}) multimode tellurite fiber (3Dp-MM-Te-fiber), thereby improving gain across these key telecommunication bands. Experiments were conducted with various pump energy levels at 980 nm and signal at 1550 nm, while the temperature varying from 20 to 120 °C in a 30 cm of heated 3Dp-MM-Te-fiber. In this framework, two opposite effects were clearly observed, i.e. (i) increasing the temperature, the peak power around 1070 nm (Yb^{3+} band) decreased, accompanied by a redshift and spectral narrowing; (ii) nevertheless, in the peak power around 1535 nm (Er^{3+} band), an increase, blueshift, and a broad in the spectrum occurs (REs-dopants), due to the increase in the temperature, resulting in enhanced amplification at 1550 nm and broadband covering the C-, L-, and U- telecommunication bands simultaneously, i.e, from approximately 1500 up to 1650 nm.

Optics EXPRESS

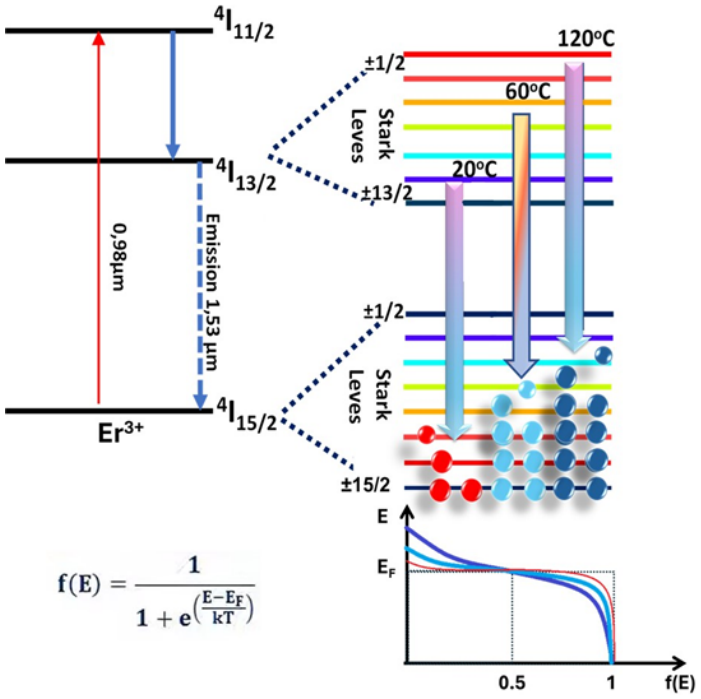

Fig. 1. Energy levels and Stark levels for the Er^{3+} ion. A pictorial representation of the electron population distribution in the Stark levels as a temperature function considering Fermi-Dirac distributions.

2. Experimental

2.1. Multimode fiber fabrication

The preform was fabricated via modified built-in-casting, as presented by [19], in the compositions 70 TeO_2 - 8.5 WO_3 - 5.5 La_2O_3 – 16 ZnO (mol%) for the cladding and 70 TeO_2 - 10.35 WO_3 – 16 ZnO – 1.0 Er_2O_3- 0.15 Tm_2O_3 – 2.5 Yb_2O_3 (mol%) for the core. Considering the differential scanning calorimetry (DSC) results, both glasses (cladding and core) exhibit good thermal stability (Tx-Tg) of about 130 °C. Therefore, we ensure a stable state and avoid the risk of crystallization in the fiber drawing process [20]. Considering the refractive index difference (Δn) observed in the bulk glasses, where both the cladding and core were made separately using the prism-coupled method, the fiber core sizes were designed to support multi-mode propagation with a numerical aperture of 0.18. Homogenous glass samples with 3.65 mol% of RE have been prepared without crystallization. High-quality optical fiber was successfully produced by drawing at a temperature of approximately 360 °C. The resulting fiber, with an external diameter of 125 µm and the cladding refractive index $n_{clad} = 2.033$, aligns with the core size of commercial silica multimode fibers, featuring an 80 µm core diameter with refractive index $n_{core} = 2.041$, ensuring effective light coupling. Scanning electron microscope (SEM) micrograph in Fig. 2 reveals a very smooth and uniform core and core-cladding interface boundary.

The transversal section of the cleaved 3Dp-MM-Te-fiber in Fig. 2, characterized by an 80 µm core diameter, allows for the propagation of the fundamental mode (LP_{01}) with a simulated effective index of $n_{eff} \approx 2.04$, as well as high-order modes at 1550 nm, which, notably, underscoring the fiber's capacity to optimize modal propagation, reduce nonlinear effects, and increase the number of data-transmitting channels [21].

Optics EXPRESS

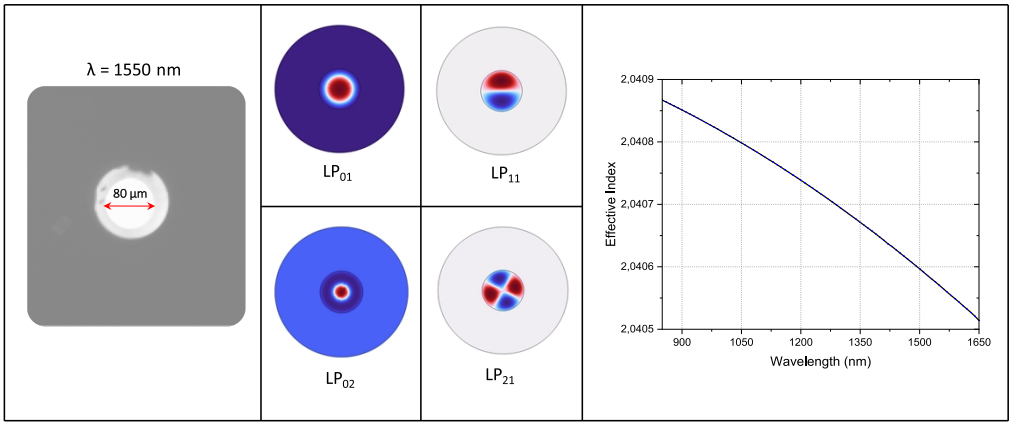

Fig. 2. Transversal section of cleaved 3Dp-MM-Te-fiber with 80 µm core diameter. Simulated fundamental and first-high order modes in 1550 nm. The effective index of LP_{01} versus wavelength.

2.2. *Thermal setup of the doped tellurite fiber*

The temperature effects in the tri-doped fiber were evaluated using a custom-built resistive heating system, including the temperature controller, as shown in Fig. 3. A pump-laser in 980 nm (BWT Diode Laser System 25 W) and a signal-laser in 1550 nm (Lightel LTS-2000 1550 nm 0.5 mW.) were injected in a 2×1 Multimode-WDM (WD9850BA - 980 nm / 1550 nm WDM, HI1060 Fiber). The built 30 cm heater system operating from 20 to 120 ^{o}C holding the Tri-doped fiber was positioned between the WDM output and the input OSA (optical spectrum analyzer — Yokogawa AQ6370D 600 ~ 1700nm).

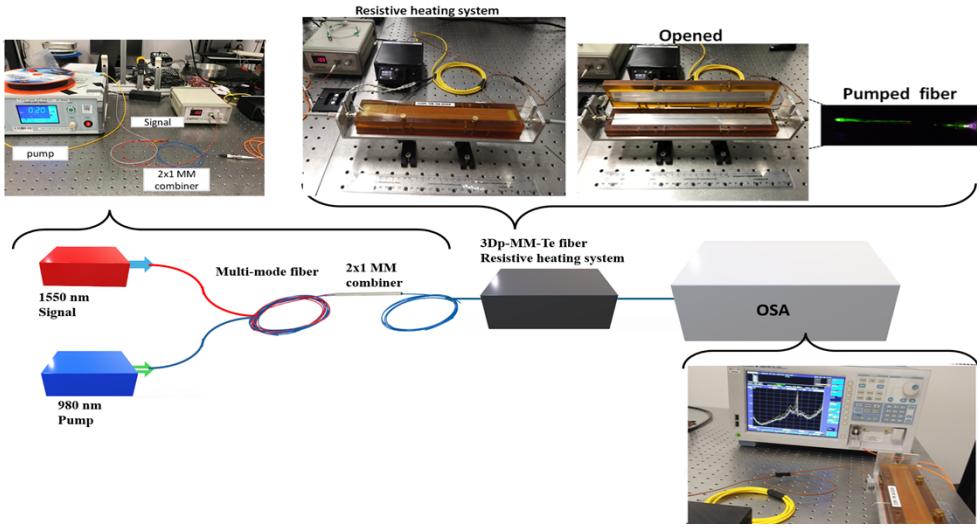

Fig. 3. Thermal experimental setup of the doped tellurite fiber. The 980 nm pump power varied from 0.1 to 3.0 W and the 1550 nm emission signal varied from 0.1 to 0.5 mW. The temperature was adjusted from 20 to 120 ^{o}C. Upper zooms highlight the resistive heating system, showing it in closed and opened positions and the green lights characteristic of the tri-doped-MM-Te-fiber pumped at 980 nm.

Optics EXPRESS

3. Results and discussions

To perform the experimental measurements of the temperature effect in the produced 3Dp-MM-Te, we used the T-MM-connectors via the ST-ST adaptor coupler (Fig. 3). This face-to-face connection introduced losses of up to 50 dB in our system, which could potentially impact overall performance. A possible explanation for this loss is the significant difference in the refractive indices (n) of the WDM (silicon fiber) and the tellurite fiber (with a $\Delta n > 0.8$). Additionally, the core diameter of the WDM is approximately 60 µm, while the tellurite fiber is 80 µm, which may also contribute to losses in the excitation of the tridoped fiber. Despite this, our research aim is to demonstrate that heating the 3Dp-MM-Te fiber can effectively broaden and amplify the signal, achieving a reconfigurable NIR emission through precise thermal control, even with the inherent losses. We carefully considered these system losses in our final analysis, determining that their impact was primarily on the sensitivity amplitude of the signal received by the optical spectrum analyzer (OSA), rather than on the fundamental efficacy of the tri-doping mechanism itself.

The first experiment focused on pumping the 30 cm of 3Dp-MM-Te fiber at 980 nm to assess its luminescence performance. We investigated the intensity of the emitted light at three different temperatures: 20, 60, and 120 °C. This systematic evaluation presented in Fig. 4, aimed to understand how varying temperatures influence the fiber's luminescent properties, providing insights into its potential applications in telecommunications and other optical technologies. We performed luminescence decay measurements on bulk glass (core preform), observing a decay time of approximately 4.3 ± 0.2 ms at 1535 nm and 3.9 ± 0.2 ms at 1790 nm. These relaxations are attributed to the single Er^{3+} and Tm^{3+} ions, respectively, and both reveal a single exponential decay.

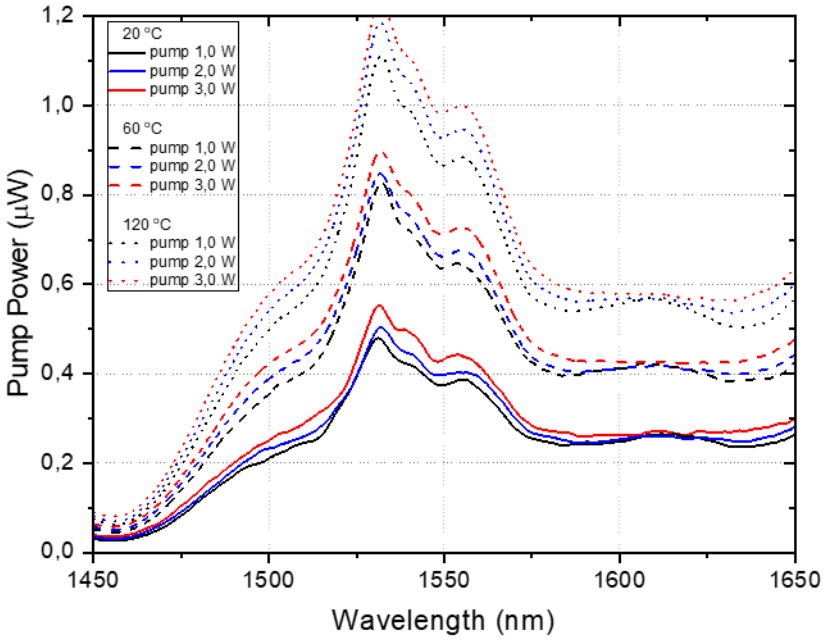

Fig. 4. Pump power intensity versus wavelength for temperature variation 20 °C solid line, 60 °C dotted line, and 120 °C dashed line, for three different pump power: 1,0 W (black), 2,0 W (blue), and 3,0 W (red)-fiber pumped at 980 nm.

In principle, under 980 nm pumping, the NIR emission intensities and broadband in Er^{3+}-dopant increase as temperature increases [13] accompanied by changes in the emission lineshape and a redshift. Observations were also verified for Er^{3+} ions in a tri-doped tellurite glass

Optics EXPRESS

[10]. Nevertheless, at lower temperatures, there is an increase in the population of Tm^{3+}:($^3F_4$), consequently high-intensity emission at 1798nm, and higher depopulation of Er^{3+}:($^4I_{13/2}$), hence low-intensity emission at 1535 nm. However, this process is also responsible for increasing the emission band, thus covering the L and U bands. Contrariwise, here, raising the temperature enhances the emission of Er^{3+} ions, driven by energy transfer from Yb^{3+} ions. Therefore, the emission intensity of Er^{3+} in the tri-doped glasses is favored by higher temperatures. In addition, the presence of Yb^{3+} ions provides sufficient energy to preserve the population inversion in both Er^{3+} and Tm^{3+} levels Stark of $^4I_{13/2}$ and $^3F_4$, respectively, keeping gain in the NIR regions as well as a broadband emission covering, in practice, all C-L and U telecommunications bands. Besides, the addition of other dopants in tellurite glasses can reduce the excited-state absorption (ESA) probability, due to competition between energy transfer and ESA processes of the states involved in such processes [10,22], thus an improvement in the NIR emission.

In a strict sense, when the temperature increases, the lower Stark levels are populated more rapidly, followed by a sequential filling of higher Stark levels, i.e. the electron population reaches all the energy sublevels as temperature increases both for Er^{3+}:$^4I_{13/2}$ and Tm^{3+}:$^3F_4$ states, see for example Fig. 1. Here, the Yb^{3+}:$^2F_{5/2}$ energy level plays a crucial role by rapidly replenishing the population of excited ions Er^{3+}:$^4I_{11/2}$ and Tm^{3+}:$^3H_5$ energy levels thus, turning the inversion population processes more efficient in both. On the other hand, high-energy pumping can also generate a large amount of heat loss in the fiber and heat dissipation boundary conditions on the fiber surface, resulting in an uneven temperature distribution in the medium. At the same time, the irregular temperature distribution in the medium may induce thermal stress which affects the fiber's mechanical properties [23]. Then, considering the results, all the experimental measurements were performed below the glass transition temperature of the fiber (T_g approximately 290°C), and with a pump power laser of no more than 3 W. Based on these experimental conditions, we will be limited to produce just thermal modifications in the electronic populations, i.e., better electrons spread in the energy sublevels of the Yb^{3+} ($^2F_{5/2}$), Tm^{3+} ($^3F_4$), and Er^{3+} ($^4I_{13/2}$) ions, achieving a reconfigurable NIR-emission gain via a thermal engineering strategy in the non-equilibrium states.

Figure 5 includes the luminescence measurements performed at different temperatures for the 3Dp-MM-Te fiber. Pumping at 980 nm and increasing the temperature, the Yb^{3+} emission levels from $^2F_{5/2} \rightarrow {}^2F_{7/2}$ occur (as shown in 1050 nm). This behavior is also observed pumping at different power densities from 0.1 to 1.0 W. However, a blueshift is observed for the Tm^{3+} from $^3F_4 \rightarrow {}^2H_6$, and Er^{3+} ions emission from $^4I_{13/2} \rightarrow {}^4I_{15/2}$. Therefore, even at room temperature (20 °C), we may note a band emission increase due to energy transfer among Er^{3+}, Tm^{3+}, and Yb^{3+}. The presence of Tm^{3+} ions plays a key role in providing flat gain in all analyzed spectrums up to 1550 nm (Er^{+} amplifier), efficiently covering the C-, L-, and U- telecommunication bands with merely 30 cm of 3Dp-MM-Te fiber. Moreover, besides the gain, as the temperature increases, we observe both a redshift around 1050 nm and a blue-broadband increment center at 1550 nm, driven by changes in electronic population distribution across the Stark levels, as illustrated in Fig. 5.

Using a 1550 nm laser, we measured the output power (peak power at 1550 nm) as a function of input power at various operating temperatures. At a fixed operating temperature, increasing the input power results in a corresponding rise in output power. Furthermore, raising the operating temperature (20, 60, and 120 °C) enhances the output power within the fiber, as illustrated in Fig. 6. Such enhancement is due to the RE dopants in the 3Dp-Te-MM fiber as well as the effects of temperature. For example, when the input power increases from 0.1 mW to 0.5 mW at an operating temperature of 20 °C, the peak power rises from -38.67 dBm (0.14 μW) to -32.81 dBm (0.52 μW), corresponding to an enhancement of approximately 5.8 dB. Similarly, with the input power fixed at 0.1 mW, increasing the operating temperature from 20 to 60 °C and then from 60 to 120 °C results in peak power increases of 1.53 dB and 1.57 dB, respectively. These observations

Optics EXPRESS

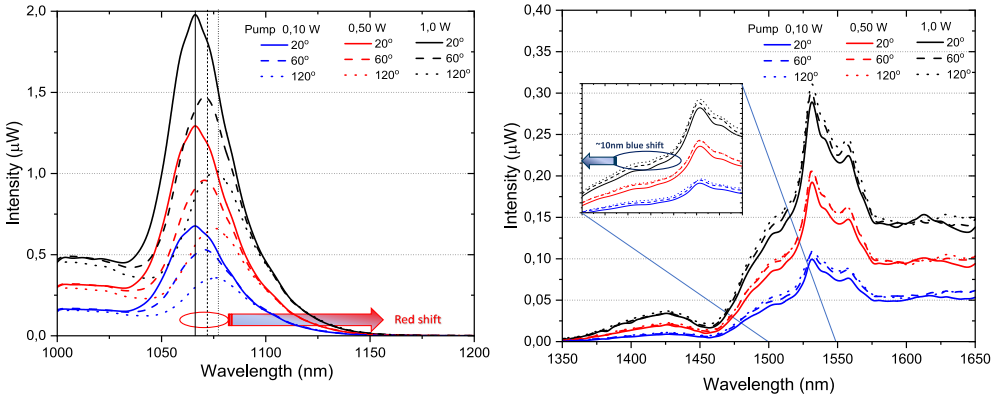

Fig. 5. Emission intensity versus wavelength for temperature variation 20 ^{o}C solid line, 60 ^{o}C dotted line, and 120 ^{o}C dashed line, for three different pump power: 0.1, 0.5, and 1.0 W. (a) Yb^{3+} emission region, and (b) the tri-doped emission region covering the C-, L-, and U-telecommunication bands. Each spectrum was measured 5 times, 10 minutes, to guarantee the repeatability of the experiment (thermal stability of the fiber under work conditions).

highlight the influence of thermal effects on enhancing peak power. This temperature dependence suggests a strong interplay between the spontaneous and stimulated emission channels inside the fiber due to the Er^{3+} dopant. Additionally, thermal excitation could facilitate energy transfer among those RE, favoring stimulated emission.

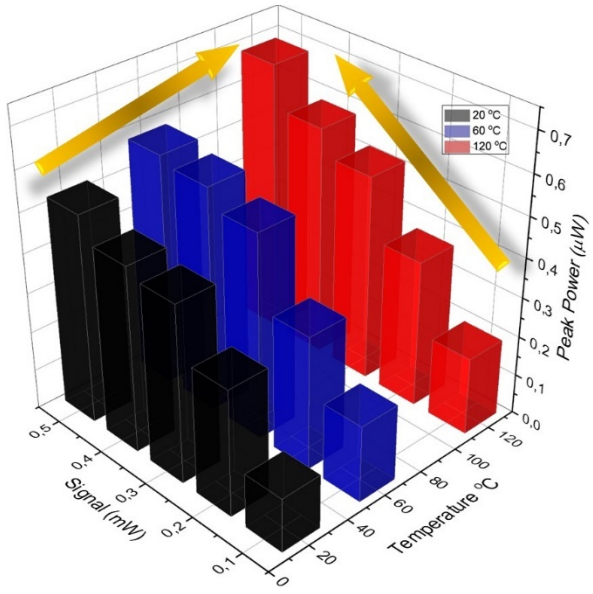

Fig. 6. The effects of temperature (20 (black), 60 (blue), and 120 ^{o}C (red)) and signal power variations (0.1, 0.2, 0.3, 0.4, and 0.5 mW) on the output peak power for 1550 nm signal transmission. Arrows inset show the increased trend.

Figure 7 presents the optical gain measurements of the 3Dp-Te-MM fiber, obtained by varying the input signal power at 1550 nm under different optical pump powers at 980 nm across three

Optics EXPRESS

operating temperatures. The results demonstrate that, under these experimental conditions, the fiber's gain performance improves significantly, see the inset Table. Furthermore, the energy transfers between the donor (Yb^{3+} and Er^{3+}) and acceptor (Er^{3+} and Tm^{3+}) of tri-dopant elements, enhance the amplification in the C-band and also contribute to a significant broadening of the wavelength-division multiplexing (WDM) spectrum into the L- to U-bands.

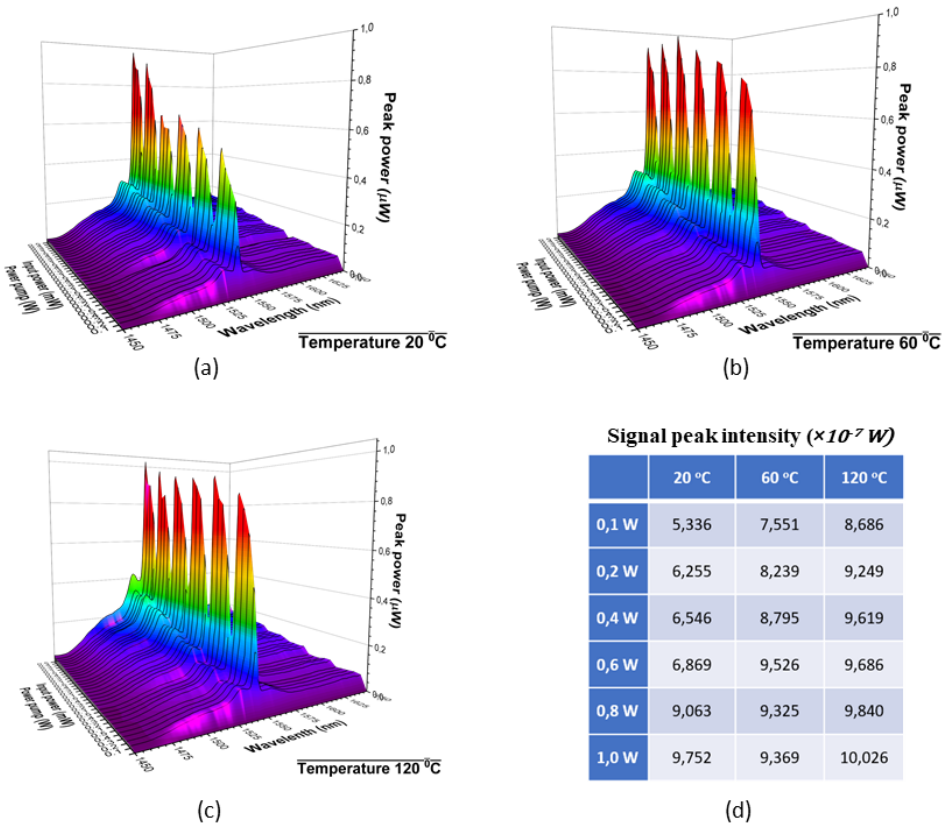

Signal peak intensity ($\times 10^{-7}$ W)

	20 °C	60 °C	120 °C
0,1 W	5,336	7,551	8,686
0,2 W	6,255	8,239	9,249
0,4 W	6,546	8,795	9,619
0,6 W	6,869	9,526	9,686
0,8 W	9,063	9,325	9,840
1,0 W	9,752	9,369	10,026

(d)

Fig. 7. Spontaneous and stimulated emission spectra under 980 nm and 1550 nm lasers. Peak power signal intensity at 1546 nm (maximum intensity registered) versus a power pump with 0.1, 0.2, 0.4, 0.6, 0.8, and 1.0 W at 980 nm, for temperature in Figure (a) 20 °C, (b) 60 °C, and (c) 120 °C. Here the input power laser signal is 0.1 up to 0.5 mW signal centered at 1546 nm. Figure (d) Table shows the intensity peak centered at 1546 nm as a function of power pumping and temperature

It is worth noting that extending amplification up to 1625 nm, covering the L-band, surpasses the conventional range of EDFAs and represents a commercially appealing approach, as it enhances the capacity of optical fiber systems [24,25]. As shown in Fig. 7, our tellurite fiber exhibits a flat emission profile across the C and L bands. This enhancement in the fiber's output signal is primarily attributed to rare-earth (RE) doping, which extends the bandwidth and increases emission intensity, enabling the simultaneous transmission of more channels. Additionally, this performance is further improved by increasing the operating temperature. For instance, in addition to the expanded broadband resulting from electronic population inversion at higher Stark levels, a temperature increase of 100°C significantly extends the C-band, causing a blueshift of approximately 10 nm. In this context, since DWDM channels can be allocated at intervals of 0.4 nm (50 GHz), 0.8 nm (100 GHz), or 1.6 nm (200 GHz), this 3Dp-Te-MM fiber enables the transmission of a greater number of signals using a single optical amplifier.

Optics EXPRESS

Furthermore, temperature control enhances the relative optical gain, as illustrated in Fig. 8. For example, when operating the 1550 nm laser at -10 dBm, an intensity increase of approximately 2.0 dB is observed as the temperature rises from 20 °C to 60 °C, and a further increase of 2.5 dB occurs as the temperature increases from 60 °C to 120 °C.

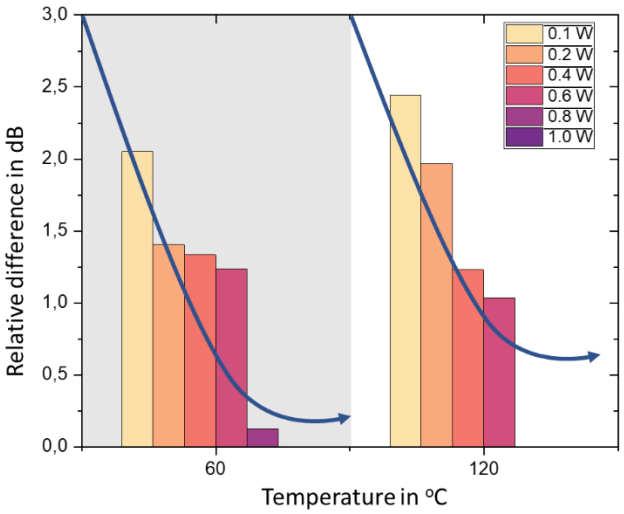

Fig. 8. Peak power intensity difference in dB relative to 20° C in 1550 nm-Signal for pumping power with 0.1, 0.2, 0.4, 0.6, 0.8, and 1.0 W, heating the 3Dp-MM-Te-fiber to 60 ° C and 120 ° C.

The Er^{3+} ions concentration plays a crucial role in preventing saturation of the short fiber amplifier (30 cm), not only in response to pumping power but also concerning heating temperature and energy transfer processes involving other rare-earth ions, as displayed in Fig. 8. In this framework, the specific combination of dopants—Er^{3+}, Tm^{3+}, and Yb^{3+}— optimizes the performance of the fiber amplifier, enhancing signal integrity and reliability for telecommunication applications. Consequently, this approach has the potential to unlock new opportunities for signal transmission and amplification of large data volumes in the telecommunications industry, enabling the use of short tellurite fibers with reduced pump power consumption.

4. Conclusions

The tri-doped (Er^{3+}-Tm^{3+}-Yb^{3+}) multimode tellurite fiber (3Dp-MM-Te-fiber) has been manufactured. We demonstrate that effective thermal population control in 30 cm of the tellurite fiber can significantly amplify and broaden the emission across the C-, L-, and U- telecommunication bands. Our findings reveal that increasing the temperature induces a blue shift around 1530 nm, while energy transfer among the rare-earth dopants results in a flat gain in the NIR region, extending from 1550 nm to 1650 nm. Notably, pumping the fiber at 980 nm with a 0.1 mW signal at 1550 nm achieves an experimental relative gain of approximately 2.5 dB at a heating temperature of 120 °C. These results highlight the potential of this tri-doped tellurite fiber reconfigurable amplifier to enhance data transmission efficiency in telecommunication systems. Additionally, it offers a solution to the spatial dimension and power consumption constraints of optical fibers versus information transmission capacity.

Funding. Conselho Nacional de Desenvolvimento Científico e Tecnológico (CNPq - process 174213/2023-9 and 402093/2022-4); Centro de Pesquisas em Óptica e Fotônica (CePOF) - São Paulo - Brazil (process 314505/2021–0); Canadian Excellence Research Chair program (CERC); Natural Sciences and Engineering Research Council of Canada; Fonds de Recherche Québecois sur la Nature et les Technologies (FRQNT); Canadian Foundation for Innovation (CFI).

Optics EXPRESS

Acknowledgments. This research was supported by the Conselho Nacional de Desenvolvimento Científico e Tecnológico (CNPq - process 174213/2023-9 and process 402093/2022-4), and through the Centro de Pesquisas em Óptica e Fotônica (CePOF) - São Paulo - Brazil (process 314505/2021–0). Besides the Canadian Excellence Research Chair program (CERC) in Photonics Innovations, the Discovery Grant program of the Natural Sciences and Engineering Research Council of Canada (NSERC), the Fonds de Recherche Québecois sur la Nature et les Technologies (FRQNT), and the Canadian Foundation for Innovation (CFI).

Disclosures. The authors declare no competing interests.

Data availability. Data underlying the results presented in this paper are not publicly available at this time but may be obtained from the authors upon reasonable request.

References

1. C. Ranaweera, C. Lim, Y. Tao, *et al.*, "Design and deployment of optical x-haul for 5 G, 6 G, and beyond: progress and challenges [Invited]," J. Opt. Commun. Netw. **15**(9), D56–D66 (2023).
2. T. Pfeiffer, "Next generation mobile fronthaul and midhaul architectures [Invited]," J. Opt. Commun. Netw. **7**(11), B38–B45 (2015).
3. A. Mori, "Tellurite-based fibers and their applications to optical communication networks," Journal of the Ceramic Society of Japan **16**, 1040–1051 (2008).
4. R. El-Mallawany, *Tellurite Glass Smart Materials: Applications in Optics and Beyond*, (Springer, 2018).
5. B. Xu, C. Jin, J.-S. Park, *et al.*, "Emerging near-infrared luminescent materials for next-generation broadband optical communications," InfoMat **6**(8), e12550 (2024).
6. V. A. G. Rivera and D. Manzani, *Technological Advances in Tellurite Glasses: Properties, Processing, and Applications*. (Springer, 2017).
7. C. Li, L. Zhu, D. Zhao, *et al.*, "Broadband NIR radiative transitions in Er^{3+}/Tm^{3+} co-doping tellurite glass material," Mater. Res. Bull. **158**, 112042 (2023).
8. V. A. G. Rivera, Y. Ledemi, M. El-Amraoui, *et al.*, "Control of the radiative properties via photon-plasmon interaction in $Er^{\wedge 3+}$-$Tm^{\wedge 3+}$-codoped tellurite glasses in the near infrared region," Opt. Express **22**(17), 21122 (2014).
9. L. Xia, Y. Zhang, J. Ding, *et al.*, "$Er^{3+}/Tm^{3+}/Nd^{3+}$ tri-doping tellurite glass with ultra-wide NIR emission," J. Alloys Compd. **863**, 158626 (2021).
10. I. C. Pinto, V. A. G. Rivera, R. Falci, *et al.*, "Tailoring near-infrared luminescence with $Er^{3+}/Tm^{3+}/Yb^{3+}$ tri-doped tellurite glasses for applications in the C, L and U bands," J. Lumin. **265**, 120206 (2024).
11. "PhysRevB.16.10".
12. X. Wang, Q. Liu, P. Cai, *et al.*, "Excitation powder dependent optical temperature behavior of Er3 + doped transparent Sr0.69La0.31F2.31 glass ceramics," Opt. Express **24**(16), 17792–17804 (2016).
13. V. A. G. Rivera, I. C. Pinto, R. Falci, *et al.*, "Novel insights into the electronic and optical properties of the 1.53-μm emission in Er^{3+}-doped oxide- and oxyfluoride- tellurite glasses for optical communications," J. Alloys Compd. **976**, 173182 (2024).
14. V. B. Pawade, V. Chopra, and S. J. Dhoble, "Introduction to electronic spectroscopy of lanthanide, properties, and their applications," in *Spectroscopy of Lanthanide Doped Oxide Materials* (Elsevier Inc., 2020), pp. 1–20.
15. N. Jaba, H. B. Mansour, and B. Champagnon, "The origin of spectral broadening of 1.53 μm emission in Er^{3+}-doped zinc tellurite glass," Opt. Mater. **31**(8), 1242–1247 (2009).
16. I. Jlassi, H. Elhouichet, M. Ferid, *et al.*, "Study of photoluminescence quenching in Er^{3+}-doped tellurite glasses," Opt. Mater. **32**(7), 743–747 (2010).
17. Y. Yang, Z. Yang, P. Li, *et al.*, "Dependence of optical properties on the composition in Er^{3+}-doped $xNaPO_3$-(80 - x)TeO_2-10ZnO-10Na_2O glasses," Opt. Mater. **32**(1), 133–138 (2009).
18. W. J. Chung and Y. G. Choi, "Local environment modification of Er^{3+} ion in tellurite glasses induced by MoO_3," J. Am. Ceram. Soc. **93**(5), 1432–1436 (2010).
19. A. Maldonado, M. Evrard, E. Serrano, *et al.*, "TeO_2-ZnO-La_2O_3 tellurite glass system investigation for mid-infrared robust optical fibers manufacturing," J. Alloys Compd. **867**, 159042 (2021).
20. N. Manikandan, A. Ryasnyanskiy, and J. Toulouse, "Thermal and optical properties of TeO 2-ZnO-BaO glasses," J. Non-Cryst. Solids **358**(5), 947–951 (2012).
21. P. Béjot, "Efficient multimode vectorial nonlinear propagation solver beyond the weak guidance approximation," J. Opt. Soc. Am. B **41**(5), 1160 (2024).
22. H. Zhu, W. Xu, Z. Fan, *et al.*, "Er^{3+}/Yb^{3+} Co-Doped Fluorotellurite Glass Fiber with Broadband Luminescence," Sensors **24**(16), 5259 (2024).
23. S. Nur Azrie Bt Safri, M. T. H. Sultan, M. Jawaid, *et al.*, "Damage analysis of glass fiber reinforced composites," in *Durability and Life Prediction in Biocomposites, Fibre-Reinforced Composites and Hybrid Composites* Elsevier, 2019, pp. 133–147.
24. C. Lei, H. Feng, Y. Messaddeq, *et al.*, "Investigation of C-band pumping for extended L-band EDFAs," J. Opt. Soc. Am. B **37**(8), 2345–2352 (2020).
25. S. Jalilpiran, V. Fuertes, J. Lefebvre, *et al.*, "Baria-Silica Erbium-Doped Fibers for Extended L-Band Amplification," J. Lightwave Technol. **41**(14), 4806–4814 (2023).